APL MATERIALS **2**, 086105 (2014)

Reversible piezomagnetoelectric switching in bulk polycrystalline ceramics

T. Stevenson,[1,a] J. Bennett,[1] A. P. Brown,[1] T. Wines,[1] A. J. Bell,[1]
R. I. Smith,[2] and T. P. Comyn[1]
[1]*Institute for Materials Research, University of Leeds, Leeds LS2 9JT, United Kingdom*
[2]*ISIS Neutron Facility, Rutherford Appleton Laboratory, Didcot OX11 0QX, United Kingdom*

(Received 22 June 2014; accepted 15 August 2014; published online 28 August 2014)

Magnetoelectric (ME) coupling in materials offer tremendous advantages in device functionality enabling technologies including advanced electronic memory, combining electronic speed, and efficiency with magnetic robustness. However, low cost polycrystalline ME materials are excluded from most commercial applications, operating only at cryogenic temperatures, impractically large electric/magnetic fields, or with low ME coefficients (1-100 mV/cm Oe). Despite this, the technological potential of single compound ME coupling has continued to drive research into multiferroics over the last two decades. Here we show that by manipulating the large induced atomic strain within the polycrystalline, room temperature multiferroic compound $0.7BiFeO_3$–$0.3PbTiO_3$, we can induce a reversible, piezoelectric strain controlled ME effect. Employing an *in situ* neutron diffraction experiment, we have demonstrated that this *piezomagnetoelectric* effect manifests with an applied electric field >8 kV/mm at the onset of piezoelectric strain, engineered in to the compound by crystallographic phase mixing. This produces a remarkable intrinsic ME coefficient of 1276 mV/cm Oe, due to a strain driven modification to the oxygen sub-lattice, inducing an increase in magnetic moment per Fe^{3+} ion of $+0.142\ \mu_B$. This work provides a framework for investigations into strain engineered nanostructures to realize low-cost ME devices designed from the atoms up, as well as contributing to the deeper understanding of single phase ME coupling mechanisms. [http://dx.doi.org/10.1063/1.4894070]

Particular attention has been given to bismuth ferrite ($BiFeO_3$)[1,2] pertaining to its room temperature ferroelectric (FE) ($T_C = 1100$ K)[2] and G-type antiferromagnetic (AFM) ($T_N \sim 643$ K)[2] properties, where the linear ME effect[2] is prohibited in the bulk due to an incommensurate magnetic structure[3] inherent to the rhombohedrally distorted (R3c) perovskite crystal structure. Polycrystalline $BiFeO_3$ is also difficult to synthesize as a pure perovskite when employing conventional mixed oxide methods, and is ferroelectrically "hard".[4] This combined with suffering from low electrical resistivity makes electrical characterization challenging.[4] Attempts to supress electrical conductivity or modify the magnetic modulation to allow linear ME coupling have been reported by employing chemical substitution, a magnetic field or inducing epitaxial strain, predominantly in thin films.[5,6]

$BiFeO_3$ forms a solid solution with the highly tetragonally distorted perovskite lead titanate ($PbTiO_3$, space group P4mm), to produce $xBiFeO_3$–$(1\text{-}x)PbTiO_3$ or BFPT.[7,8] This addition stabilizes the perovskite phase and increases the electrical resistivity to allow FE and piezoelectric characteristics to be measured across the compositional space.[9] The BFPT compound remains rhombohedral from $1 \geq x > 0.7$, whereas for $x < 0.7$ the equilibrium crystal structure is tetragonal. This phase transformation is analogous to the morphotropic phase boundary (MPB)[10] observed in the

[a]Electronic mail: t.j.stevenson@leeds.ac.uk.

commercially dominant piezoelectric (Pb,Zr)TiO_3 (PZT).[11] At the x = 0.7 crystallographic phase boundary, ferroelectric and antiferromagnetic R3c ordering remains up to T_C = 908 K[7] and $T_N \sim$ 560 K[8], respectively, while the tetragonal P4mm phase T_N = 220 K.[12] An 80 K drop in T_N of the R3c antiferromagnetic phase between 1 > x > 0.7 is commensurate with the 30% dilution of the magnetic Fe^{3+} ions by diamagnetic Ti^{4+} on the B-site whereas the 340 K drop in T_N between phases at the x = 0.7 boundary is purely structural in origin. It is interesting to note that the T_N of the two phases span ambient temperature.

The tetragonal phase exhibits a large spontaneous crystallographic strain (lattice parameter ratio c/a-1) of 19% for unclamped particles.[7,10] This is larger than most epitaxial films and > 3 times that observed in the $PbTiO_3$ end member alone (6%),[13] hence polycrystalline ceramics of this composition are subject to large intergranular stresses as crystallites are constrained upon cooling through the FE Curie temperature. Phase transformation of a fraction of the crystallites to the lower volume R3c symmetry results, establishing a broad region of antiferromagnetic R3c and paramagnetic P4mm phase coexistence between 0.4 < x < 0.7[8,10] at ambient temperature. By engineering an MPB, we are able to maximize the potential for electric field-induced ferroelectric switching, by balancing the phase content to achieve a moderate coercive field and lattice distortion, something that cannot be achieved in either phase fraction alone,[11] and within a compound that also contains magnetically ordered ions (Fe^{3+}).

This subsequently offers an electrically driven lattice distortion which will directly influence the magnetic ion. Whereas in non-magnetic MPB PZT, the maximum proportion of domain switching is observed at ~50% tetragonal phase content,[14] the spontaneous strain of the BFPT compound is much higher, and therefore we anticipate that the rhombohedral content required to achieve practical switching strains in BFPT should also be higher than in PZT.

Thus the x = 0.7 composition, with 89% rhombohedral phase content,[15] offers a unique opportunity to examine the discontinuities in the 3 ferroic order parameters, electric polarization, strain and magnetization, as a function of applied stress, electric, and magnetic fields at ambient temperatures.

A key aspect of the work presented here is the use of neutron diffraction as this allows the determination of the atomic arrangement, strain, and magnetic dependencies simultaneously to characterize all 3 ferroic order parameters as a function of electric field (*E*). Diffraction enables this to be achieved without artefacts from ferroelectric or magnetic domains, grain boundaries, or other material discontinuities. This work contributes to a deeper understanding of single compound ME materials mechanisms, a requirement identified by Eerenstein *et al.*[16] in a review of the field.

Powder of x = 0.7 x$BiFeO_3$–(1-x)$PbTiO_3$ was fabricated using conventional mixed oxide methods (>99.9% purity) as described previously.[8] Powder was uniaxially and isostatically pressed to 100 MPa and 400 MPa, respectively, prior to sintering at 1273 K and cooling (20 K/h) to form dense polycrystalline bulk ceramics, 30 mm in diameter. The discs were mechanically thinned and polished to 600 μm and electroded on both sides with silver.

Our measurements were performed repeatedly on discs of the x = 0.7 BFPT material, with the highest resolution data presented here from the Polaris neutron diffraction instrument. Time of flight neutron diffraction data were collected in the 6 fixed angle detector banks of the Polaris instrument at the ISIS pulsed spallation neutron source, Rutherford Appleton Laboratory (RAL), UK.[17] An electric field was applied parallel to the incident beam across aluminium spring pins used to affix the sample to a bespoke cryostat sample stick with boron nitride electrical insulation (see Fig. 1 of the supplementary material).[18] To prevent electrical breakdown, the modified stick was placed within a cryostat and evacuated to $< 5.0 \times 10^{-5}$ mbar to prevent arcing, whilst cooled to 250 K ($\pm$ 1°). This relatively small drop in temperature saw the effect of increasing sample resistivity by a factor of 10^4 to allow a greater field to be achieved over long periods of time with negligible modifications to phase contributions, strain, or magnetic arrangements.[15] Diffraction data were collected over all detector banks at 4 h periods per step in voltage, applying an effective field of 0–11 kV/mm.

Whole pattern structure refinement is inappropriate for *in situ* diffraction measurements under electric field due to crystallographic texture and anisotropic strain induced during poling. Instead least squares profile fitting of the individual peaks has been employed using WinPlotR, part of the FullProf suite.[19] The use of such software allows the peaks to be modelled and a calculation of position and integrated intensity extracted.

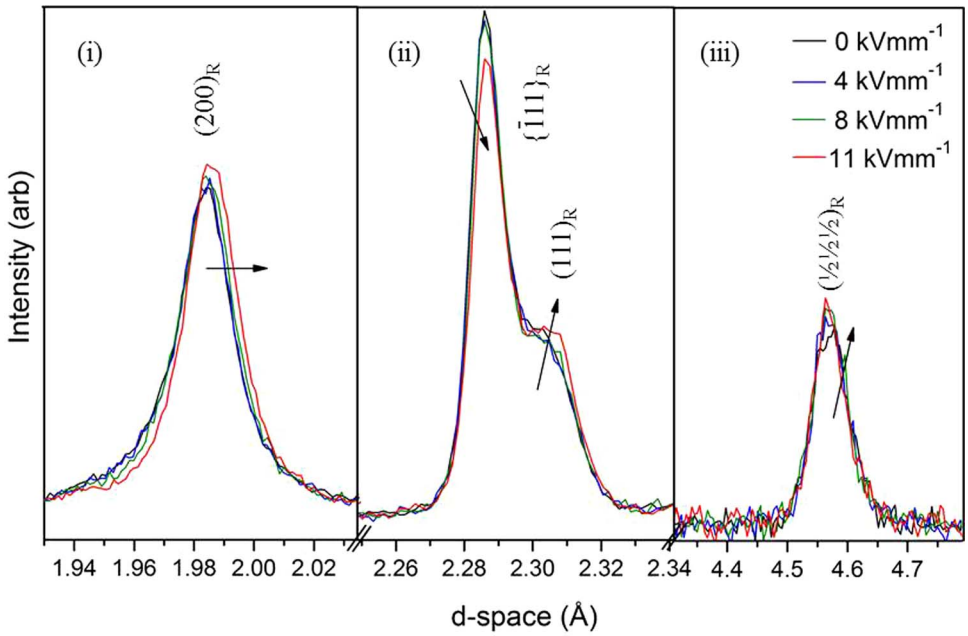

FIG. 1. Diffraction pattern of polycrystalline BFPT x = 0.7 collected from the Polaris instrument, illustrating the effect of the application of electric field from 0 (black) to 11 (red) kV mm^{-1} on the (i) $(200)_R$, (ii) $\{111\}_R$, and (iii) antiferromagnetic reflections. Data are shown from bank 6 (i), 6 (ii), and 3 (iii), respectively.

At the conclusion of the experiment, the piezoelectric charge coefficient "d_{33}" was measured in direct mode employing a commercial Berlincourt meter at 110 Hz.

At 4.6 Å in the resulting diffractogram, the rhombohedral phase $(^1/_2{}^1/_2{}^1/_2)_R$ (in pseudo cubic space) purely AFM magnetic plane is observed (Figure 1). This corresponds to a magnetic propagation vector (k) parallel to the pseudocubic $<111>_R$ or equivalent $<001>_H$ for the hexagonal setting.[8,20]

Indexing the diffraction pattern (see Figure 2 of the supplementary material)[18] confirms the co-existence of rhombohedral R3c and tetragonal P4mm symmetries as expected.[8] Applying peak analysis techniques from Hall *et al.*[21,22] gives the ratio of these phases calculated from the integrated intensities of the respective $\{110\}_R$ and $\{101\}_T$ families of peaks (see Figure 3 of the supplementary material)[18] and reveals a rhombohedral phase fraction = 89.1%. This is in excellent agreement with previous Rietveld structure refinements for this composition.[15] A combined oxygen sub-lattice tilt with a magnetic contribution $(^3/_2{}^1/_2{}^1/_2)_R$ peak was revealed at ∼2.4 Å,[8] and additional peak at ∼2.35 Å was attributed to the silver electrode (Fm3 m̄ space group). Modifications of the $(200)_R$, $\{110\}_R$, and $\{111\}_R$ peaks, as a function of applied electric field parallel to the neutron beam, show increasing lattice shift and integrated intensities for $0 \leq E \leq 11$ kV/mm (Figure 2). Above a critical field of 8 kV mm^{-1}, we observe magnetic and piezoelectric coupled phenomena.

The neutron diffraction data collected show a polycrystalline sample of x = 0.7 BFPT undergoes three separate field-dependent atomic re-ordering mechanisms as a function of applied electric field which result in a reversible *piezomagnetoelectric* response.

Increasing E causes a linear increase in the calculated fraction of rhombohedral-tetragonal phase to 97.8% R3c at 8 kV/mm. This significant transformation of ∼8% of the paramagnetic tetragonal phase to the AFM rhombohedral symmetry results in a 7.6% linear increase in antiferromagnetic peak intensity (Figure 2). Electric field driven phase transformations are seen in other systems, including from tetragonal in the ubiquitous piezoelectric PZT (<4 kV/mm)[14] and in thin films of the $BiFeO_3$ end member[23] as a stress relief mechanism. This mechanism is observed elsewhere upon application of hydrostatic pressure,[24] and fits well with the data presented here, indicating that the field-induced intergranular stresses are relieved by partial transformation from tetragonal to the ∼5% lower volume rhombohedral unit cell. This is achieved by rotation of the polar axis from $<001>_T$ to

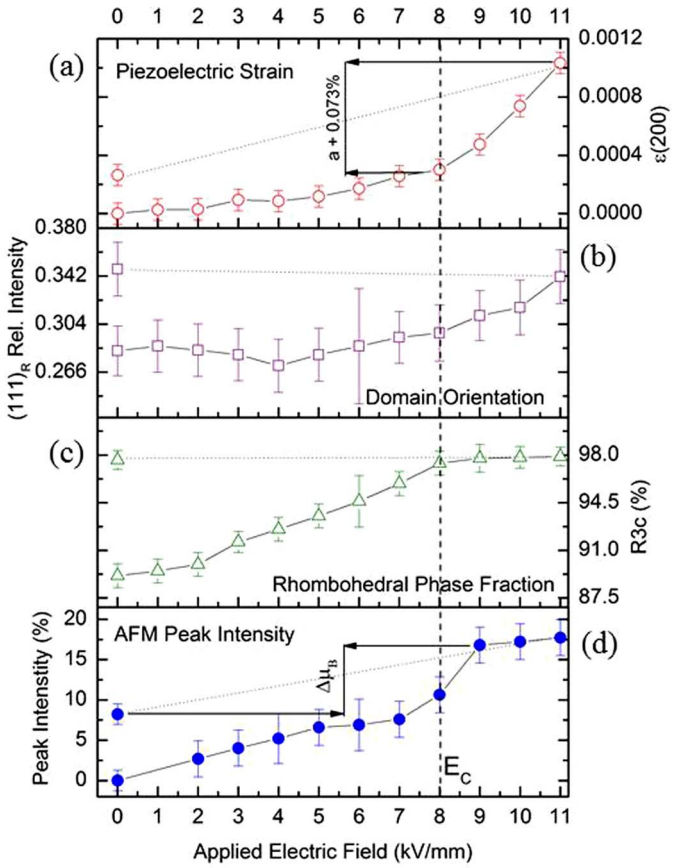

FIG. 2. Variation in (a) $\varepsilon(200)$ strain, (b) calculated intensity of the $(111)_R$ relative to the $((1\bar{1}1)_R$, $(1\bar{1}1)_R$, and $((\bar{1}\bar{1}1)_R$, (c) calculated R3c phase fraction, and (d) antiferromagnetic peak intensity (4.6Å) as a function of increasing electric field, and with the field off. Error bars represent least squares fit (σ) standard deviation from WinPlot R peak fitting model.

$<111>_R$ (Figure 3). Above this critical field of 8 kV/mm, however, this stress relief transformation appears to cease, and on removal of the electric field is non-reversible.[24]

The $(200)_R$ reflection shift, a representation of the $a/2$ lattice parameter strain $\epsilon(200)$, and its response to E reveals that above the critical field of 8 kV/mm, and until 11 kV/mm, a reversible 0.073% strain occurs in the a lattice parameter. This is indicative of the intrinsic piezoelectric effect occurring in the rhombohedral unit cell (Figure 2 and 3). This piezoelectric "transition" at 8 kV mm^{-1} is the coercive field (E_c) and is commensurate with PZT, where phase transformations are preceded by piezoelectric strain, but occurs to a lesser degree in BFPT due to the greater degree of tetragonality (c/a) instilled in the compound.[14] As the coercive field is exceeded, the movement of the B-site Fe and Ti ions distorts the surrounding oxygen octahedra. This is illustrated in Figure 4 and Table I, where the E field dependence of the ($^3/_2$, $^1/_2$, $^1/_2$) reflection, a contribution of the oxygen FeO_6 sub-lattice nuclear and magnetic peaks, indicates a clear discontinuity and reversible peak separation $> E_C$. This is commensurate with a modification of the oxygen octahedral tilt angle,[25] and could consequently affect the antiferromagnetic superexchange network.[26]

This critical field is also visible for changes in the $\{111\}_R$ family of planes. Above E_{crit}, the $(111)_R$ increases in intensity as the combined intensity of the 3 equivalent planes $((1\bar{1}1)_R$, $(1\bar{1}1)_R$, and $((\bar{1}\bar{1}1)_R)$ decrease (Figure 1). This is attributed to domain re-orientation in the rhombohedral phase, resulting in an increase from the ~3:1 peak ratio[21] at 0 kV/mm (Figure 2). As the phase transformation desists, domain switching occurs in the established rhombohedral phase for those unit cells orientated in any of the 3 polar directions not already parallel to the E field $<111>_R$ (Figure 3). Again this is common amongst ferroelectric materials, with domain orientation occurring in PZT

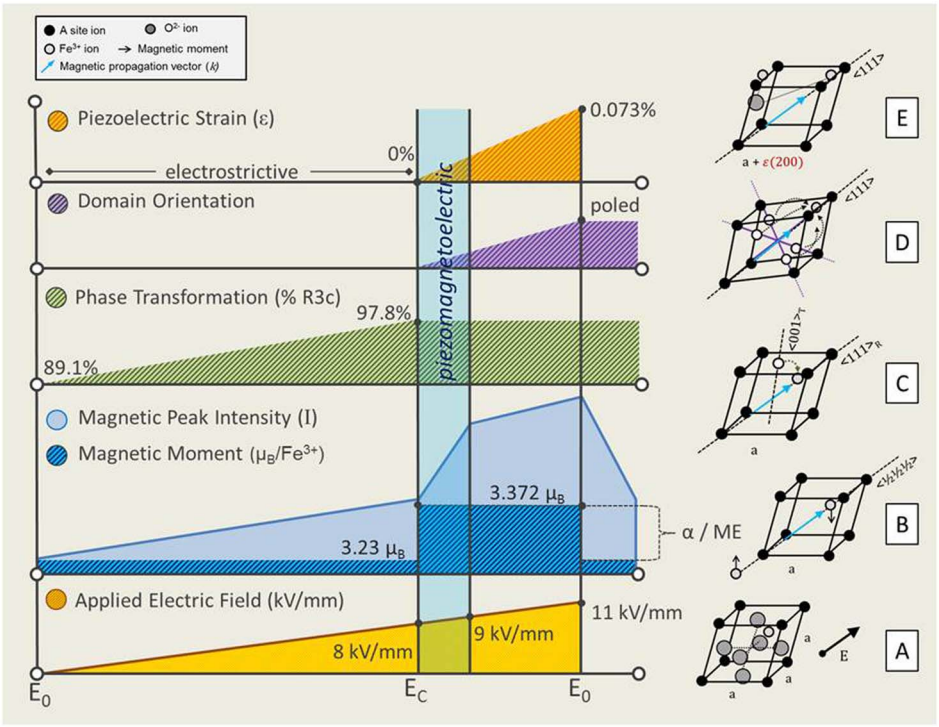

FIG. 3. Exaggerated schematic summarizing the varying mechanisms leading to observed changes in magnetic order for BFPT with increasing electric field. The effect of (a) electric field on the (b) magnetic peak intensity and moment, (c) tetragonal to rhombohedral phase transformation, (d) domain orientation to the <111>, and (e) piezoelectric strain is shown with respect to the Fe-O-Fe network.

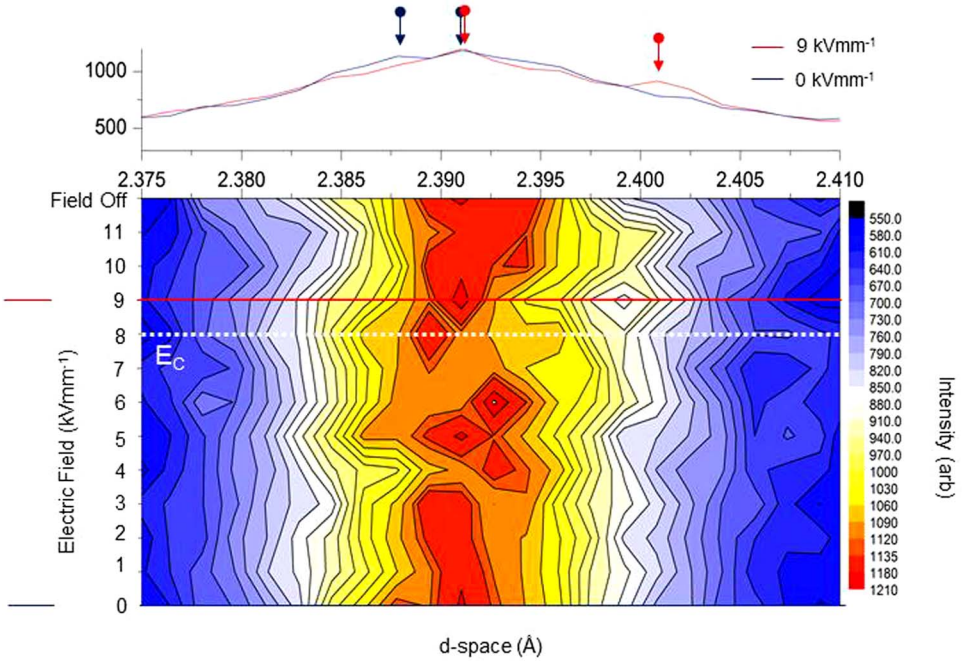

FIG. 4. Plot of the $(^3/_2,^1/_2,^1/_2)_R$ reflection, a combination of oxygen sub-lattice nuclear and magnetic contributions at 0 kV mm^{-1} and 9 kV mm^{-1} (peaks labelled with arrow), from diffraction data (top) and an intensity contour plot of the $(^3/_2,^1/_2,^1/_2)_R$ peak at 0 to 11 kV mm^{-1} and return to 0 kV/mm (bottom).

TABLE I. Peak position and full width half maximum (FWHM) calculated for the $(^3/_2,^1/_2,^1/_2)_R$ reflection from peak fitting, a combination of oxygen sub-lattice nuclear and magnetic contributions at 0 kV mm^{-1} to 11 kV mm^{-1}. Difference from initial 0 kV mm^{-1} is shown in brackets.

Electric field/kV mm^{-1}	Peak position/Å	FWHM
0	2.3911 (+0.0000)	0.0174 (+0.0000)
3	2.3912 (+0.0001)	0.0186 (+0.0012)
6	2.3911 (+0.0000)	0.0193 (+0.0019)
9	2.3915 (+0.0004)	0.0215 (+0.0041)
11	2.3930 (+0.0019)	0.0213 (+0.0039)
Return to 0	2.3913 (+0.0002)	0.0182 (+0.0008)

(<1 kV/mm).[14] The effect is less pronounced and requires significantly larger E fields in BFPT, as the material is ferroelectrically harder and consequently more difficult to pole.[9] On removal of the E field domain orientation is observed to be retained, and a piezoelectric coefficient $d_{33} = 2.3$ pC/N was subsequently recorded. The onset of reversible piezoelectric strain, limited domain orientation and piezoelectric performance is in excellent agreement with previous electrical characterization performed on the same composition, which determined an observed critical field as the ferroelectric coercive field $E_C = E_{crit} = 8$kV/mm.[9]

The domain orientation contributes to a small linear increase in magnetic peak intensity at >9 kV/mm (Figure 2), because of the increase in magnetic Fe^{3+} ions that are aligned along the $<111>_R$ direction and consequently contributing to diffraction in the $(^1/_2{}^1/_2{}^1/_2)_R$ antiferromagnetic plane.

The discontinuity in rhombohedral antiferromagnetic peak intensity $(^1/_2{}^1/_2{}^1/_2)_R$ at $7 < E \leq 9$ kV/mm is observed to occur simultaneously with E_C, and is similarly observed to be reversible to the same degree (Figure 2). Modelling of the mechanisms which can contribute to intensity changes in the AFM reflection was completed for Fe^{3+} ions with a $x = 0.7$ occupancy, in BFPT, within an R3c space group utilizing the General Structure Analysis System (GSAS) software.[27] Above E_C, as there is no longer any modification to the magnetic volume incurred from phase transformation, any changes can be shown to be a result of manipulating the magnetic moment per Fe^{3+} ion within the compound (see Figure 4 of the supplementary material).[18] Thus for the diffraction experiment presented here, the 9.5% reversible intensity variation, measured from 9 kV/mm to the removal of E for the AFM peak (Figure 2), relates to a substantial change in the magnetic moment per Fe^{3+} ion of 0.142 μ_B.

Changes in the magnetization of ME materials have been observed throughout the literature as a consequence of applying stress, magnetic field, and chemical substitution. In $BiFeO_3$, this tends to be reported as any one of these methods destroying the incommensurate AFM order,[8] allowing ferromagnetic ordering to persist and subsequently allowing the linear ME effect to exist.[6] For BFPT presented here, the mechanism appears to be exceptionally different. Although we can establish a direct correlation with the lattice distortion, and incommensurate order is known to exist in the compound,[8] any switching to the FM state would require the AFM peak to disappear and for the nuclear Bragg peaks to be enhanced with FM contributions. This is clearly not observed, and hence precludes any magnetomechanical effects or spin-spin interaction for FM ions.[26,28]

Instead, at $\sim E_C$ we propose a *piezomagnetic* response,[29] whereby the immediate onset of strain causes the magnetic moment to increase via the enhancement in antiferromagnetic interaction strength. A possible mechanism is that lattice strain occurs, imparting tensile strain in the $<111>_R$ direction to the unit cell, modifications to the Fe^{3+}-O-Fe^{3+} geometry[20] ensues, providing dimensional modifications to the antiferromagnetic superexchange network.[26] This also facilitates subsequent, yet limited domain orientation (Figure 4). Although the lattice strain prevents resolving the $(^3/_2{}^1/_2{}^1/_2)_R$ reflection oxygen and magnetic components, gross modifications such as discontinuous peak shift, splitting, and broadening is seen > 8 kV/mm (Figure 4, Table I) which is indicative of oxygen octahedral variations.[25] This re-alignment of the super-exchange network quickly saturates the spin-lattice coupling,[26] and consequently a linear relationship between the piezoelectric strain and magnetization does not extend beyond 9 kV/mm. Instead the magnetic interaction reaches a new

energetically favourable ground state for the same magnetic ion. The increase in magnetic moment due to proposed superexchange modifications is in keeping with similar observations elsewhere on increasing the $BiFeO_3$ content[25] or reducing the temperature in BFPT[3]. As the E field is removed, the Fe^{3+} and O^{2-} ions accede to thermal agitation and relax back to the pre coercive field lattice condition, returning the μ_B/Fe^{3+} to its original ground state, without transformation back to the tetragonal phase and while retaining the poled domain configuration.

Although the experiment is taken on a bulk AFM polycrystalline sample, the use of diffraction allows an atomic scale view of the system. Applying this rationale to ME coupling, these results infer an effective linear ME coefficient (α) for the x = 0.7 rhombohedral unit cell over the applied electric field $\Delta E = 9$ kV/mm (Figure 4), of ME_E $\alpha_{111} = 1699$ ps/m (equivalent to $\alpha = \varepsilon dE/dM = 1276$ mV/cm Oe where $\varepsilon_r = 120$ for x = 0.7). This order of magnitude increase compared to equivalent single compound materials is exceptional and proportionate to particulate ME composites in the literature.[30] This is driven by the same stress interface methodology that has been applied to composites but at the unit cell, rather than grain boundary scale.

In conclusion, 3 separate mechanisms have been shown to contribute to the E field induced changes in magnetization of polycrystalline $0.7BiFeO_3$–$0.3PbTiO_3$ (Figure 3) with all being dependent on the crystallographic structure. First lower fields cause a partial ferroelectric-ferroelectric phase transformation < 8 kV mm^{-1}, inducing a larger volume of R3c which can sustain a greater volume of AFM order. Above 8 kV/mm, domain switching aligns more magnetic Fe^{3+} ions in the observation direction $<111>_R$ combined with the onset of intrinsic piezoelectric strain. This onset of piezoelectric strain causes a significant change in the spin-lattice coupling to saturate the magnetic interaction strength, stimulating a reversible increase in magnetic moment per Fe^{3+} ion. An effective ME coefficient is therefore determined to be an order of magnitude larger than other single phase bulk polycrystalline ME materials and operates well above cryogenic temperatures. Although it is expected to require fields in excess of 8 T to observe the inverse effect through a piezomagnetic strain induced electrical polarization, there is still an exciting prospect and enormous scope for designing devices that employ moderate electric fields around E_C on thin ceramic sections to activate the magnetically sensitive piezomagnetoelectric state. For example, the magnitude of the electric field induced magnetization could be exploited in a FM-AFM coupled device as an electric field induced shift in the magnetic exchange bias would enable the production of single compound memory technologies.

We acknowledge support from EPSRC under the Doctoral Training Grant scheme and STFC for provision of neutron beam time at the ISIS facility.

[1] M. Fiebig, J. Phys. D: Appl. Phys. **38**, R123 (2005).
[2] G. Catalan and J. F. Scott, Adv. Mater. **21**, 2463 11 (2009).
[3] P. Fischer, M. Polomska, I. Sosnowska, and M. Szymanski, J. Phys. C: Solid State Phys. **13**, 1931 (1980).
[4] T. Rojac, M. Kosec, B. Budic, N. Setter, and D. Damjanovic, J. Appl. Phys. **108**, 074107 (2010).
[5] R. Ramesh and N. A. Spaldin, Nat. Mater. **6**, 21 (2007).
[6] J. Wang, J. B. Neaton, H. Zheng, V. Nagarajan, S. B. Ogale, B. Liu, D. Viehland, V. Vaithyanathan, D. G. Schlom, U. V. Waghmare, N. Spaldin, K. M. Rabe, M. Wuttig, and R. Ramesh, Science **299**, 1719 (2003).
[7] V. V. S. S. Sai Sunder, A. Halliyal, and A. M. Umarji, J. Mater. Res. **10**, 1301 (1995).
[8] T. Stevenson, T. P. Comyn, A. Daoud-Aladine, and A. J. Bell, J. Magn. Magn. Mater. **322**, L64 (2010).
[9] T. P. Comyn, T. Stevenson, and A. J. Bell, J. Phys. **128**, 13 (2005).
[10] V. Kothai, A. Senyshyn, and R. Ranjan, J. Appl. Phys. **113**, 084102 (2013).
[11] H. Kungl and M. J. Hoffmann, Acta Mater. **55**, 5780 (2007).
[12] T. P. Comyn, T. Stevenson, M. Al-Jawad, G. André, A. J. Bell, and R. Cywinski, J. Magn. Magn. Mater. **323**, 2533 (2011).
[13] Y. Matsuo and H. Sasaki, J. Am. Ceram. Soc. **48**, 229 (1966).
[14] K. Schönau, M. Knapp, H. Kungl, M. Hoffmann, and H. Fuess, Phys. Rev. B **76**, 144112 (2007).
[15] T. P. Comyn, T. Stevenson, M. Al-Jawad, S. L. Turner, R. I. Smith, W. G. Marshall, A. J. Bell, and R. Cywinski, Appl. Phys. Lett. **93**, 232901 (2008).
[16] W. Eerenstein, N. Mathur, and J. Scott, Nature (London) **442**, 759 (2006).
[17] S. Hull, R. Smith, W. David, A. Hannon, J. Mayers, and R. Cywinski, Physica B: Condens. Matter **180–181**, 1000 (1992).
[18] See supplementary material at http://dx.doi.org/10.1063/1.4894070 for the experimental setup of the Polaris experiment; for complete diffraction patterns collected on Polaris; for an example of a WinPlot peak fitting profile; and for a antiferromagnetic diffraction peak intensity model.
[19] J. Rodriguez-Carvajal, Physica B: Condens. Matter **192**, 55 (1993).
[20] R. Ranjan, V. Kothai, A. Senyshyn, and H. Boysen, J. Appl. Phys. **109**, 063522 (2011).

[21] D. A. Hall, T. Mori, P. J. Withers, H. Kungl, M. J. Hoffmann, and J. Wright, Mater. Sci. Technol. **24**, 927 (2008).
[22] D. A. Hall, A. Steuwer, B. Cherdhirunkorn, P. Withers, and T. Mori, Ceram. Interfaces **34**, 679 (2008).
[23] R. J. Zeches, M. D. Rossell, J. X. Zhang, A. J. Hatt, Q. He, C.-H. Yang, A. Kumar, C. H. Wang, A. Melville, C. Adamo, G. Sheng, Y.-H. Chu, J. F. Ihlefeld, R. Erni, C. Ederer, V. Gopalan, L. Q. Chen, D. G. Schlom, N. A. Spaldin, L. W. Martin, and R. Ramesh, Science **326**, 977 (2009).
[24] T. P. Comyn, T. Stevenson, M. Al-Jawad, W. G. Marshall, R. I. Smith, J. Herrero-Albillos, R. Cywinski, and A. J. Bell, J. Appl. Phys. **113**, 183910 (2013).
[25] J. Bennett, A. J. Bell, T. J. Stevenson, R. I. Smith, I. Sterianou, I. M. Reaney, and T. P. Comyn, Mater. Lett. **94**, 172 (2013).
[26] A. Millis, Nature (London) **392**, 147 (1998).
[27] A. C. Larson and R. B. Von Dreele, General Structure Analysis System (GSAS), Los Alamos National Laboratory Report LAUR 86-748 (2004).
[28] D. Bulte and R. Langman, J. Magn. Magn. Mater. **251**, 229 (2002).
[29] I. E. Dzialoshinskii, J. Exptl. Theoret. Phys. (USSR) **33**, 807–808 (1957) [Sov. Phys. JETP **33**, 807 (1957)].
[30] A. D. Sheikh, A. Fawzi, and V. L. Mathe, J. Magn. Magn. Mater. **323**, 740 (2011).